ADVANCED FUNCTIONAL MATERIALS
www.afm-journal.de

Organic Light-Emitting Physically Unclonable Functions

Nilgun Kayaci, Resul Ozdemir, Mustafa Kalay, N. Burak Kiremitler, Hakan Usta, and M. Serdar Onses**

The development of novel physically unclonable functions (PUFs) is of growing interest and fluorescent organic semiconductors (*f*-OSCs) offer unique advantages of structural versatility, solution-processability, ease of processing, and great tuning ability of their physicochemical/optoelectronic/spectroscopic properties. The design and ambient atmosphere facile fabrication of a unique organic light-emitting physically unclonable function (OLE-PUF) based on a green-emissive fluorescent oligo(*p*-phenyleneethynylene) molecule is reported. The OLE-PUFs have been prepared by one-step, brief (5 min) thermal annealing of spin-coated nanoscopic films (≈40 nm) at a modest temperature (170 °C), which results in efficient surface dewetting to form randomly positioned/sized hemispherical features with bright fluorescence. The random positioning of molecular domains generated the unclonable surface with excellent uniformity (0.50), uniqueness (0.49), and randomness ($p > 0.01$); whereas the distinctive photophysical and structural properties of the molecule created the additional security layers (fluorescence profile, excited-state decay dynamics, Raman mapping/spectrum, and infrared spectrum) for multiplex encoding. The OLE-PUFs on substrates of varying chemical structures, surface energies and flexibility, and direct deposition on goods via drop-casting are demonstrated. The OLE-PUFs immersed in water, exposed to mechanical abrasion, and read-out repeatedly via fluorescence imaging showed great stability. These findings clearly demonstrate that rationally engineered solution-processable *f*-OSCs have a great potential to become a key player in the development of new-generation PUFs.

1. Introduction

The design and development of novel encoded surfaces are of great research interest in today's world for use in anti-counterfeiting and authentication applications. Although the majority of encoded surface applications relate to the prevention of counterfeit goods (e.g., electronics, banknotes, and medicines),[1] they have an additional significance in the information age for hardware and data security, for which novel ways are still needed to develop robust authentication processes.[2,3] One common approach to prepare an encoded surface is the generation of a geometrically defined response as a result of an external challenge.[4,5] The one-dimensional barcodes used with consumer goods are one of the best-known examples of such encoded surfaces. When challenged with a scanner, the response is a well-defined array of lines completing the authentication process. An inherent limitation of this approach is, however, that the deterministic processes used during the fabrication of such geometrically defined patterning make these encoded surfaces vulnerable to third parties. A promising solution that has gained recent attention involves the exploitation of physically unclonable functions (PUFs).[6,7] In this approach, the response of the encoded surface against a challenge is determined through a physical and stochastic process.[8] This stochasticity and inherently random responses prevent the replication of encoded surfaces by third parties or even by the manufacturer itself.[9] Starting from the seminal work by Pappu et al.,[6] optical PUF systems have been an active research area.[10–17] In the past decade, a range of material types and manufacturing routes have been studied to demonstrate PUFs using silica microparticles,[6] inherent randomness of surfaces,[18,19] randomly positioned scatterers challenged by quantum states of

N. Kayaci, M. Kalay, N. B. Kiremitler, M. S. Onses
ERNAM–Nanotechnology Research and Application Center
Erciyes University
Kayseri 38039, Turkey
E-mail: onses@erciyes.edu.tr

N. Kayaci, N. B. Kiremitler, M. S. Onses
Department of Materials Science and Engineering
Erciyes University
Kayseri 38039, Turkey

The ORCID identification number(s) for the author(s) of this article can be found under https://doi.org/10.1002/adfm.202108675.

DOI: 10.1002/adfm.202108675

R. Ozdemir, H. Usta
Department of Nanotechnology Engineering
Abdullah Gül University
Kayseri 38080, Turkey
E-mail: hakan.usta@agu.edu.tr

M. Kalay
Department of Electricity and Energy
Kayseri University
Kayseri 38039, Turkey

M. S. Onses
UNAM–Institute of Materials Science and Nanotechnology
Bilkent University
Ankara 06800, Turkey

light,[20,21] carbon nanotubes,[22] spherical[23,24] and rod shaped[25] plasmonic nanoparticles, silver nanoislands,[26] core-shell nanoparticles,[27] polymeric particles,[28] diamonds,[29] and fluorescent compounds.[30]

For the development of PUFs, fluorescent compounds are particularly interesting because they allow for rapid and simple authentication with multiple and interactive challenge-response pairs using facile and well-developed spectroscopic/microscopic techniques and portable tools. Several recent demonstrations have reported the fabrication of PUF-based encoded surfaces using a few different fluorescent compounds. In an earlier work, Gooding and coworkers have used an organic dye conjugated plasmonic nanoparticles for multiplex encoding.[31] While Sorensen and coworkers[32–33] used lanthanide ions-doped materials that were randomly dispersed in a polymeric matrix, Liu et al. generated randomly positioned arrays of quantum dots and perovskite nanocrystals using an inkjet printing technique that was assisted with a surface functionalization.[34–35] In another example, Kim and coworkers fabricated fluorescent and silk proteins-based edible PUFs that can be directly attached onto the surface of medicines.[36] Addressable PUFs were reported using silk-based laser arrays with randomized lasing response.[37] Very recently, the modulation of the fluorescence intensity and lifetime for perovskite nanocrystals via metasurfaces has been demonstrated as a novel method of PUF fabrication.[38]

As far as fluorescent materials are concerned for the fabrication of PUF-based encoded surfaces, rationally designed π-conjugated organic semiconductors[39–41] could be a highly attractive material family based on their ease of synthesis and structural modification, high photoluminescence efficiency, solution-processability to form thin-films, and fingerprint-like spectral information. Precise control and tuning over their chemical structures, physicochemical (e.g., thermal transitions or solubility in a specific solvent) and photophysical (e.g., absorption/emission maxima, optical band edge, or excited-state lifetime) properties are possible to meet the specific needs of a particular application.[42] The exploratory organic synthesis of π-conjugated systems offers an extremely rich chemistry for fluorescent organic semiconductors (*f*-OSCs) with an extremely wide range of structures/properties as compared to other types of fluorescent materials.[43,44] Even a confidential *f*-OSC molecule, which has been unknown to everyone, with very specific challenge-response pairs could easily be designed and synthesized for a particular company or a consumer product. The *f*-OSC molecules could open new avenues for next-generation unique PUF-based encoded surfaces. Despite all these premises, the strong potential of *f*-OSCs in the fabrication of PUF-based encoded surfaces, especially by employing facile methods, have remained underutilized. At this point, it is noteworthy that *f*-OSCs are robust compounds both from materials development and thin-film functionality perspectives, and they have already shown great promise in electroluminescent devices[45] and sensor technologies.[46] Today, there is an increasing amount of organic light-emitting diode (OLED) displays[47] on varied commercial electronics that are fabricated using *f*-OSCs.

In this perspective, the question arises as to how randomized features could be formed by fluorescent organic semiconductors. In some recent studies, random fluorescent features were created for fluorescent π-conjugated molecules. In the first study, organic single-crystalline arrays with random sizes and dual-wavelength lasing emission properties were solution-deposited on top of topographically and chemically patterned substrates.[48] In the other study, a diarylethene-based molecule was first processed to form microparticles and then deposited on hydrophobic/hydrophilic micropatterns to afford highly integrated micro-hemisphere resonators with pixel-specific spectral fingerprints.[49] Despite these recent advancements, a desired method for practical PUF applications should not involve complicated, expensive, and time-consuming processes (i.e., lithography or printing techniques), and it should allow for rapid, direct, and simple fabrication that is applicable to large areas on various types of surfaces. To this end, it is well known that π-conjugated molecules typically show thermal transitions below 200 °C, which is well below their thermolysis onset temperatures (i.e., >300—350 °C), and their nanoscopic thin-films (thickness < 100 nm) could exhibit strong microstructural/morphological changes upon thermal treatment.[50] And, in some examples, thermal annealing on spin-coated organic semiconductor films was even found to cause the formation of discontinuous crystal grains deterring the semiconducting channel in organic transistors.[51] The temperatures required for these changes in the nanoscopic thin-films are generally below their bulk solid-state transition temperatures.[52] Therefore, nanoscopic thin-films of a rationally designed *f*-OSC offer a great potential to yield efficient surface dewetting upon thermal annealing at modest temperatures, which could enable the fabrication of randomized molecular domains with distinct photophysical properties and spectral fingerprints. We have recently demonstrated that the dewetting of poly(2-vinyl pyridine) in thin films provides a robust platform to generate PUF-based security layers.[53] To this end, oligo(*p*-phenyleneethynylene) π-frameworks stand out as an ideal *f*-OSC family for PUF applications with their favorable structural (i.e., flexible swallow-tailed alkyl chains), physicochemical (good solution-processability, low-temperature thermal transitions, and amorphous solid-state) and photophysical (efficient and unique fluorescence) properties.

Herein, we present the design and facile ambient atmosphere fabrication of organic light-emitting physically unclonable functions (OLE-PUFs) based on a green-emissive oligo(*p*-phenyleneethynylene) molecule, 1,4-bis((4″-diphenylamino-3-cyano-[1,1″-biphenyl]-4-yl)ethynyl)-2,5-bis(2-ethylhexyloxy)benzene (2EHO-TPA-CNPE, **Figure 1**a).[54] 2EHO-TPA-CNPE is a highly fluorescent molecule ($\Phi_{\text{PL-solution}} \approx 1$ and $\Phi_{\text{PL-solid state}} \approx 0.5$) showing hybridized local and charge-transfer excited state properties, and its emission profile in the spin-coated neat thin-film phase has a CIE 1976 (u'',v'') chromaticity coordinate of (0.10, 0.55) corresponding to a night vision imaging systems (NVIS) compatible Green A region. The OLE-PUFs were prepared by one-step brief (5 min) thermal annealing of spin-coated nanoscopic thin films at a modest temperature (170 °C), which results in excellent surface dewetting to form randomly positioned/sized hemispherical features with bright fluorescence. While the random positioning of molecular domains generated the unclonable surface with inherent randomness, the distinctive photophysical and structural properties of

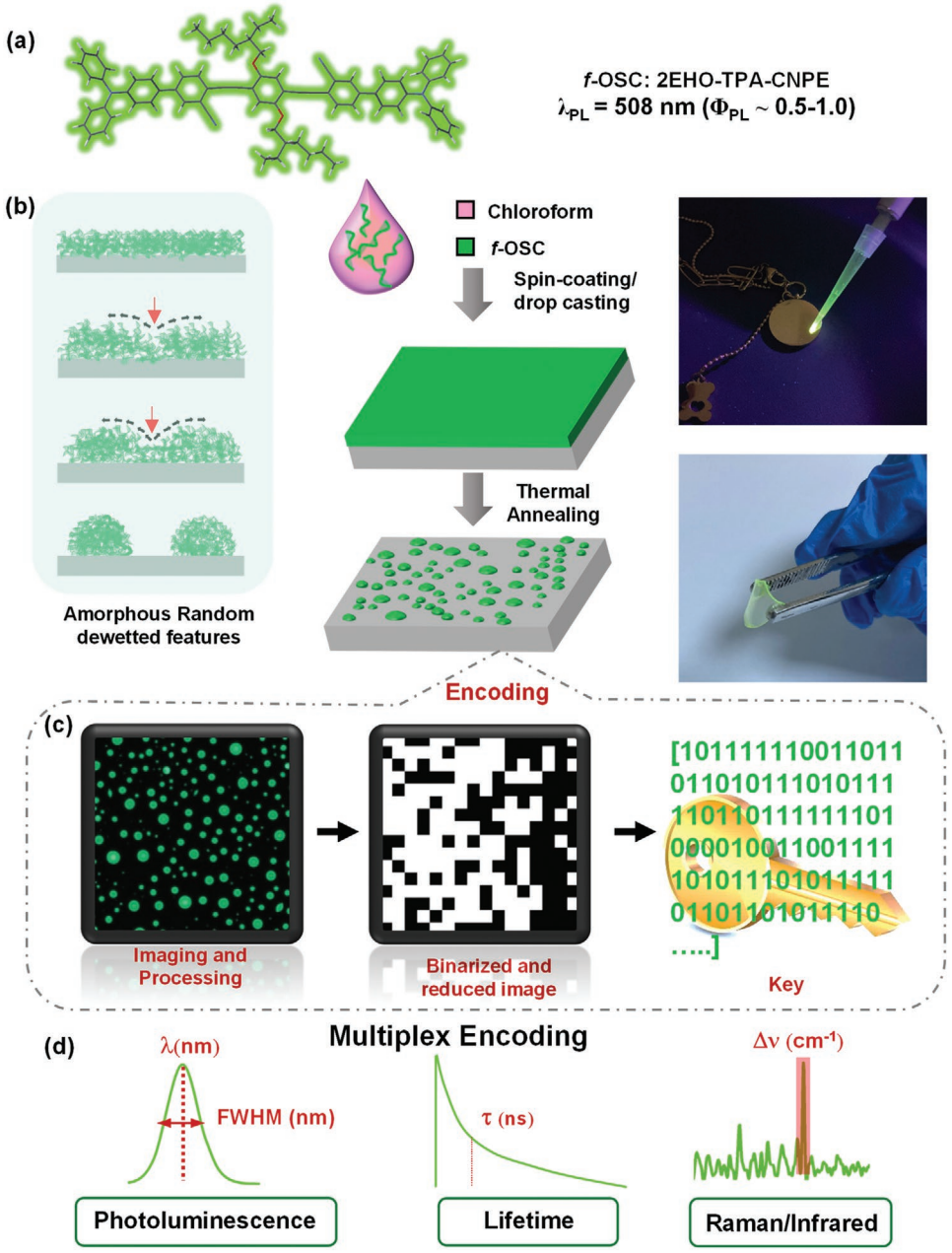

Figure 1. Schematic description for the fabrication of organic light-emitting physically unclonable functions (OLE-PUFs). a) Structure of the green-emissive fluorescent organic molecule **2EHO-TPA-CNPE** and the solid-state fluorescence emission maximum/quantum efficiency values. b) Fabrication steps for OLE-PUFs on varied substrates (bare/PS-grafted silicon, poly(vinyl chloride), and goods): the organic molecule is dissolved in chloroform and spin-coated/drop-casted on a substrate. Heating (in the ambient atmosphere or under nitrogen) results in spontaneous dewetting and the formation of randomly positioned features. c) Representative authentication process. Fluorescence microscopy images are used to construct binary images and keys. These keys can be compared with the database to verify the originality of the entity. d) Multiple additional security layers of OLE-PUFs based on photoluminescence profile, excited state decay kinetics, and Raman/Infrared spectrum.

2EHO-TPA-CNPE created the additional security layers (fluorescence profile, excited-state decay dynamics, Raman mapping/spectrum, and infrared spectrum) for multiplex encoding. The size and spacing of the random features were found to depend on the film thickness and thermal annealing conditions. The presence of 2-ethylhexyloxy's located on the central phenylene ring and the terminal triphenylamine groups does not only provide good solution-processing, but also induces an amorphous microstructure in the dewetted solid-state domains. During the formation of randomized domains, the amorphous nature further contributes to the randomness of this process. The OLE-PUFs on PS-grafted or freshly cleaned (only native oxide layer) silicon substrates, flexible substrates, and direct deposition on goods (via drop-casting) were demonstrated.

Finally, the current OLE-PUFs immersed in water, exposed to mechanical abrasion by sand, and read-out repeatedly via fluorescence imaging retained their functionality.

2. Results and Discussion

The synthesis, purification, and characterization of 2EHO-TPA-CNPE were performed in accordance with our recently reported procedure.[54] As shown in Figure 1, *f*-OSC solutions were first prepared by dissolving 2EHO-TPA-CNPE in chloroform in the ambient atmosphere at room temperature. The molecular dissolution was instantaneous due to its excellent solubility in common organic solvents, which is provided by the presence of swallow-tailed flexible 2-ethylhexyloxy substituents on the central phenylene ring and highly twisted terminal triphenylamine groups. *f*-OSC solutions were then spin-coated on polystyrene (PS) grafted silicon substrates in the ambient atmosphere at room temperature to yield nanoscopic molecular thin-films with thicknesses of ≈30-60 nm. Here, we note that our later findings (vide infra) revealed that the thin-film deposition process is adaptable to flexible plastic substrates without needing an end-grafted PS layer, and, other than spin-coating, drop-casting is also possible, which is particularly advantageous for the direct formation of OLE-PUFs on goods. Considering that 2EHO-TPA-CNPE's dimensions along the long and short molecular axes are 3.55 nm and 1.51 nm (Figure S1, Supporting Information), respectively, and the as-deposited thin-films do not have a specific molecular orientation (vide infra), there seems to be about ≈20–40 molecules deposited along the film thickness. In order to generate OLE-PUFs via spontaneous dewetting of molecular thin-films, a brief (5 min.) one-step thermal annealing was performed. Although we have initially performed this annealing in an inert atmosphere, our later experiments (vide infra) have demonstrated that the ambient atmosphere annealing is also possible, thanks to the good thermal stability and the robust chemical structure of 2EHO-TPA-CNPE. While heating above glass transition at relatively high temperatures (>200—250 °C) was typically required for the formation of dewetted structures in polymer thin films,[53,55,56] the dewetting dynamics are quite different in the case of nanoscopic molecular thin-films. The solid-state of molecular semiconductor thin-films, from the cumulative cohesive energetics perspective, are bound by relatively weak π-interactions and van der Waals forces, especially when compared with polymeric materials.[57–60] Therefore, molecular mobility and diffusion could easily become effective at a moderate temperature that is typically well below the melting temperature, and the molecular film could be disintegrated into separate domains to minimize the surface energy.[52] For 2EHO-TPA-CNPE thin-films, the formation of the first holes was observed at 100—120 °C as the beginning of film disintegration (Figures S2 and S3, Supporting Information). Note that this is well below the melting point (195 °C based on DSC) of the bulk solid-state (Figure S4, Supporting Information). With the increased temperature getting close to the melting point, the dewetting became more evident and the complete dewetting from the underlying polymeric interface to form randomly positioned hemi-spherical molecular domains occurred at a modest temperature of 170 °C. The large variations observed in the sizes of these *f*-OSC domains and in the separation distances between them offer a great advantage contributing to the randomness of these patterns. Also, the separation distances between *f*-OSC domains are in the micrometer length scale, which makes the OLE-PUFs identification via optical and spectroscopic-mapping techniques viable. The fluorescence microscopy images of the random features obtained served as the basis of our OLE-PUF design. These images are binarized and reduced to generate binary keys that consist of zeros (no fluorescence) and ones (fluorescence). In a real-world application, such keys can be attached to products and the authenticity can be verified by comparing these binary codes with the ones in the database. An inherent characteristic of OLE-PUFs is multiplex encoding (Figure 1d). While random positioning of f-OSC domains is the basis of the generation of an unclonable surface, the unique photophysical and structural properties of π-structures offer additional security layers that can be probed using different spectroscopic techniques. The fluorescence maximum and onset wavelengths, full-width-at-half-maximum (fwhm) value, and the excited state decay dynamics (i.e., exponential fit and lifetime) are highly specific to the π-structure of an organic molecule, and they all can be used as an encoding medium for the current OLE-PUFs. As a complementary security layer, 2EHO-TPA-CNPE has also a fingerprint Raman scattering and infrared spectrum. Besides the particular Raman bands, note that confocal Raman microscope setups[61] could allow mapping for the response of the system.

With the increased spin-coating solution concentration, the initial film thickness prior to thermal annealing was found to increase from 31.9 nm (for 0.1 wt.%) to 40.7 nm (for 0.2 wt.%) and 59.1 nm (for 0.4 wt.%). When these films with different thicknesses were annealed at 170 °C for 5 min, the size, height, and interstitial spacing between the formed hemi-spherical molecular domains were found to strongly depend on the initial spin-coated 2EHO-TPA-CNPE film thickness. The dewetted *f*-OSC surfaces were imaged via optical, fluorescence, and atomic force microscopy (AFM) techniques (**Figure 2**). As evidenced from these images, both the diameter and height of the hemi-spherical caps were found to increase with the initial film thickness. An increase in the film thickness, as a result of an increased number of molecular layers per unit area, reduces the nucleation density of holes upon thermal annealing and facilitates molecular diffusion to yield polygon-like large hole formations (≈200 μm in diameter) arranging the molecular features (≈10–25 μm in diameter) around these holes to form a cellular pattern. The average diameter/height (at the maximum) of the hemi-spherical caps were measured to be 1.14 μm/51.63 nm, 2.94 μm/160.84 nm, and 17.14 μm/745.79 nm, respectively. On the other hand, while relatively thicker films prepared from 0.4 wt.% solution show domain thinning at 100 °C (Figure S2, Supporting Information), thinner films prepared from 0.2 wt.% solution already show a high density of hole formation at 100 °C (Figure S3, Supporting Information). The polygon or cellular pattern structures observed for the thick films are in between regular (e.g., well-ordered crystals) and completely disordered structures (e.g., amorphous glass), and similar structures could be found in nature in soap froths, soil of deserts, and plants.[55] Apparently, increasing film thickness induces an energetic

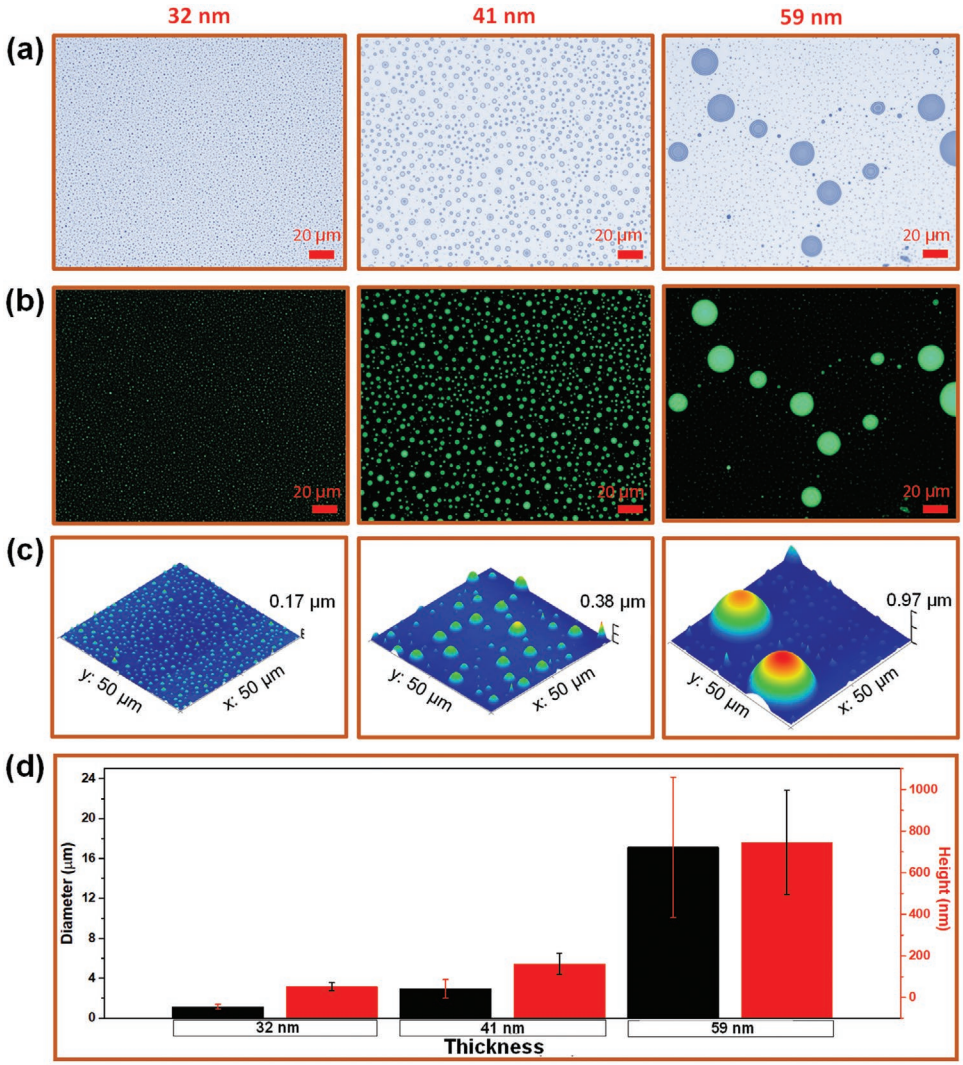

Figure 2. Effect of the film thickness on OLE-PUFs. Spin-coated films on PS-grafted substrates using *f*-OSC solutions of varying concentrations (0.1, 0.2, and 0.4 wt.%). a) Optical microscopy, b) fluorescence microscopy, and c) AFM images. d) The average diameter (in black) and height (in red) of the features as derived from the optical microscopy and AFM images, respectively.

barrier to the formation of favorable OLE-PUFs. In order to reveal the origin of the observed changes in the diameter and height of the hemi-spherical caps, we performed two control experiments. First, the morphology and crystallinity of the 2EHO-TPA-CNPE films prior to thermal annealing were probed using AFM and θ–2θ out-of-plane XRD analysis, respectively, which showed (Figure S5, Supporting Information) very similar characteristics. In a second experiment, we varied the thickness of the 2EHO-TPA-CNPE films by spin-coating the same concentration at different rotation speeds. The diameter and height of the hemi-spherical caps following thermal annealing decreased with the increased rotation speed (Figure S6, Supporting Information). These results further suggest that the thickness of the film, rather than the solution concentration of the *f*-OSC, determines the characteristics of the dewetted features. Due to high surface coverage, perfect randomness with no evident pattern formation, and easily conceivable feature sizes for optical microscopy, we choose 2EHO-TPA-CNPE-based OLE-PUFs with a thickness of ≈41 nm for the rest of this study. However, we note that the observed tuning of the *f*-OSC features via initial film thickness and annealing temperature could provide further novel ways to encode information.

To investigate the microstructural ordering in these molecular domains, the θ–2θ out-of-plane XRD scans were measured for the current OLE-PUFs. As shown in Figure S7, Supporting Information, a strong diffraction peak in the low-angle range ($\theta < 10°$), which is typically observed for thin-films of molecular π-systems, was absent. The observed featureless diffraction pattern in the $\theta = 0$–$40°$ range clearly demonstrates that the current dewetted 2EHO-TPA-CNPE domains consist of highly disordered (amorphous) molecules. The amorphous nature of the heated-cooled dewetted features is consistent with the thermal behavior of 2EHO-TPA-CNPE's bulk solid-state as characterized via differential scanning calorimetry measurement (Figure S4, Supporting Information).[54] On the other hand, when the XRD characterization was performed on the as-spin

coated semiconductor film prior to thermal annealing (Figure S7b, Supporting Information), the thin-film was again found to be amorphous indicating that 2EHO-TPA-CNPE does not crystallize from solution phase during spin-coating. During the formation of OLE-PUFs, amorphous nature of 2EHO-TPA-CNPE greatly contributes to the randomness of this process. An undesired molecular crystallinity behavior could induce preferential crystal growths in certain directions to form ordered structures, which would be expected to reduce the degree of randomness. It is noteworthy that the fluorescent molecules previously developed in our research in the oligo(*p*-phenyleneethynylene) molecular family,[54,62–63] regardless of their π-architectures and acceptor units, indeed shows a common feature of amorphous nature and no-crystallization for heated-cooled samples. Therefore, the oligo(*p*-phenyleneethynylene) molecular family, with varied structures and properties, offers a great potential for the development of OLE-PUFs consisting of randomly formed amorphous domains. The structural and excited state information encoded within the current OLE-PUFs is revealed by steady-state fluorescence and time-resolved photoluminescence decay measurements, Raman mapping, and Infrared spectrum (Figures 3 and S8, Supporting Information). The fluorescence spectrum taken directly on the OLE-PUF surface gave an emission maximum and an onset at specific wavelengths of 508 nm and 590 nm, respectively. As shown in **Figure 3**a-inset, the PL decay profile recorded at the fluorescence maximum (λ_{exc} = 375 nm and 200 ps pulse width) by the time-correlated single photon counting method showed a very unique behavior with regards to exponential fitting and lifetimes. The curve was best fitted to a three-exponential function giving two prompt lifetimes of 0.33 ns (61%) and 1.04 ns (38%) followed by a delayed PL of 5.2 ns (1%). The Raman spectrum (Figure 3b) taken over the dewetted features reveals three distinct peaks positioned at 1100 cm^{-1}, 1590 cm^{-1}, and 2200 cm^{-1} associated with –C–H, –C=C–, and –C≡N/–C≡C– groups, respectively. The Raman spectrum taken across the OLE-PUF background does not include these peaks and is rather dominated by the silicon peak positioned at ≈520 cm^{-1}. This strong contrast in the Raman spectra provides a great opportunity to generate excellent Raman mapping images for the current OLE-PUFs. In addition to excited state and fluorescence properties, this chemical information serves as an additional security layer. Here,

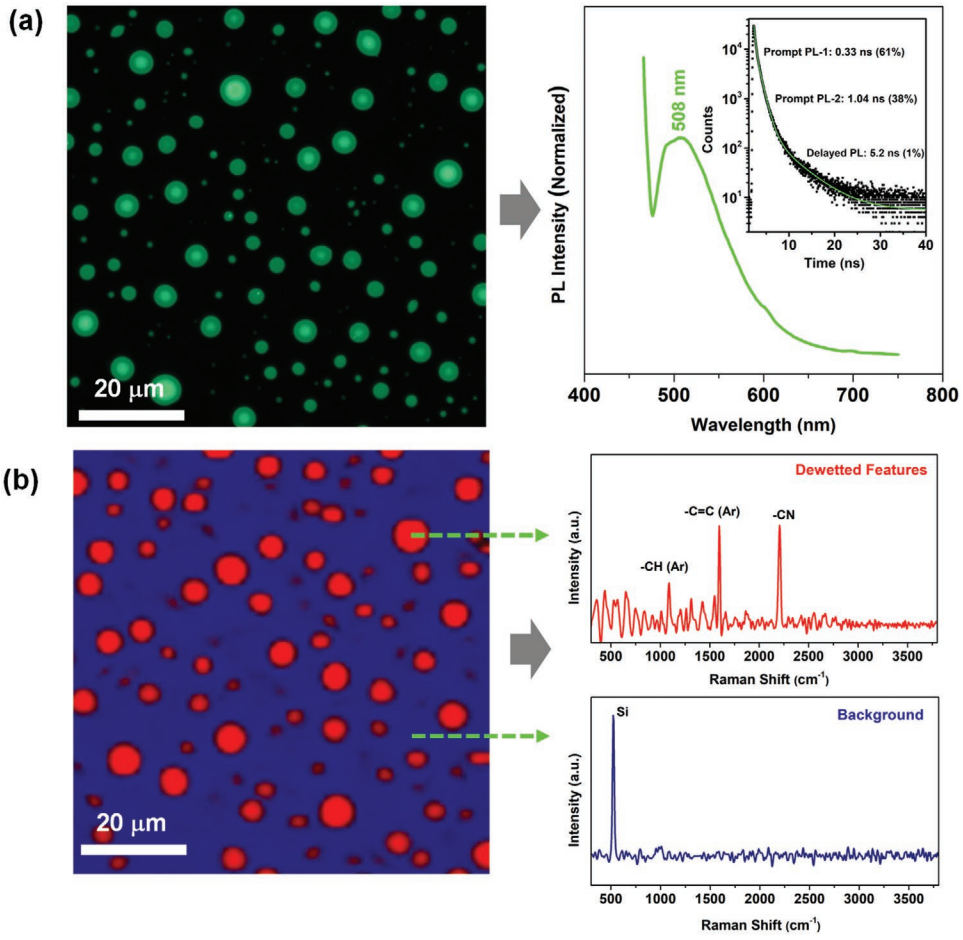

Figure 3. Photoluminescence and chemical based security layers of OLE-PUFs. a) Fluorescence microscopy image and the corresponding photoluminescence spectrum. The inset shows the transient photoluminescence decay profile with the lifetimes (prompt PL-1 and PL-2, and delayed PL) and their contributions based on a three-exponential fitting. b) Raman mapping image and Raman spectra were obtained on the dewetted features and the background regions. The mapping image was generated using the Raman band at a position of 521 cm^{-1} for blue and 1594 cm^{-1} for red color. The OLE-PUF was generated by spin-coating a 0.2 wt.% solution of *f*-OSC on the PS-grafted substrate.

it is noteworthy that the low-energy band edge of the optical absorption spectrum for 2EHO-TPA-CNPE thin-film extends to 450–500 nm. Therefore, the OLE-PUF features could be electronically excited with a relatively long wavelength eliminating the need for using higher energy (<400 nm) photons, at which a much larger number of π-systems could be excited. From a counterfeiting perspective, this reduces the chance of finding a fake fluorescent molecule if the input challenge is properly adjusted. In addition, the ATR-FTIR spectrum (Figure S8, Supporting Information) gave fingerprint-like spectral data for the current OLE-PUFs, which provides another strong barrier for the counterfeiters.

We finally investigate the performance of OLE-PUFs. To generate quantitative metrics that are commonly used as figures of merit in PUF studies, fluorescence microscopy images were first converted to security keys. For this purpose, the images were first binarized and their sizes were reduced to 16 × 16 pixels. **Figure 4**b presents a representative binarized image with a reduced size. In this image, white pixels correspond to fluorescent regions which consist of dewetted *f*-OSC. This binarized image is then used to generate 256-bits long security keys consisting of 1-bits and 0-bits. This procedure is repeated for 10 samples to generate 10 different security keys (see Figure S9, Supporting Information for the images). For each of these keys, uniformity, uniqueness, and randomness values were then calculated (see supporting information for details).[64] The uniformity is an important metric giving insights on the equal distribution of 1-bits and 0-bits. The ideal value is 0.5, showing a perfectly equal distribution of 1-bits and 0-bits, in an analogy to the probability of having heads and tails being equal in an unbiased coin. Figure 4d shows that the uniformity values are close to the ideal value with an arithmetic average of 0.503. Note that such uniformity is achieved without the use of any debiasing algorithm,[36] thanks to the high surface coverage of the dewetted features. Next, we calculate the Hamming distance values for the keys generated from 10 samples. When comparing two different chips, inter-chip Hamming distance compares two different keys and indicates the number of bits with a different value. This comparison is made for 45 combinations. The distribution of normalized inter-chip Hamming distances (i.e., Hamming distance divided by the key length) is presented in Figure 4e. The uniqueness derived from the Hamming distance values is calculated as 0.4901. This uniqueness value is close to the optimal value of 0.5, implying the ability of the current physical system to generate distinct codes. Finally, we probed the randomness of the features using frequency test.[65] The *p*-value was greater than 0.01 for each sample, further supporting the great randomness of the dewetted features (Table S1, Supporting Information). OLE-PUF exhibited remarkable levels of reliability. To simulate authentication via different imaging conditions, we took fluorescence microscopy images of a sample at 6 different exposure times ranging from 250 ms to 5000 ms (Figure S10, Supporting Information). The randomly positioned features could be clearly detected in all these different imaging conditions. These fluorescence images were then processed using a MATLAB code to generate keys.

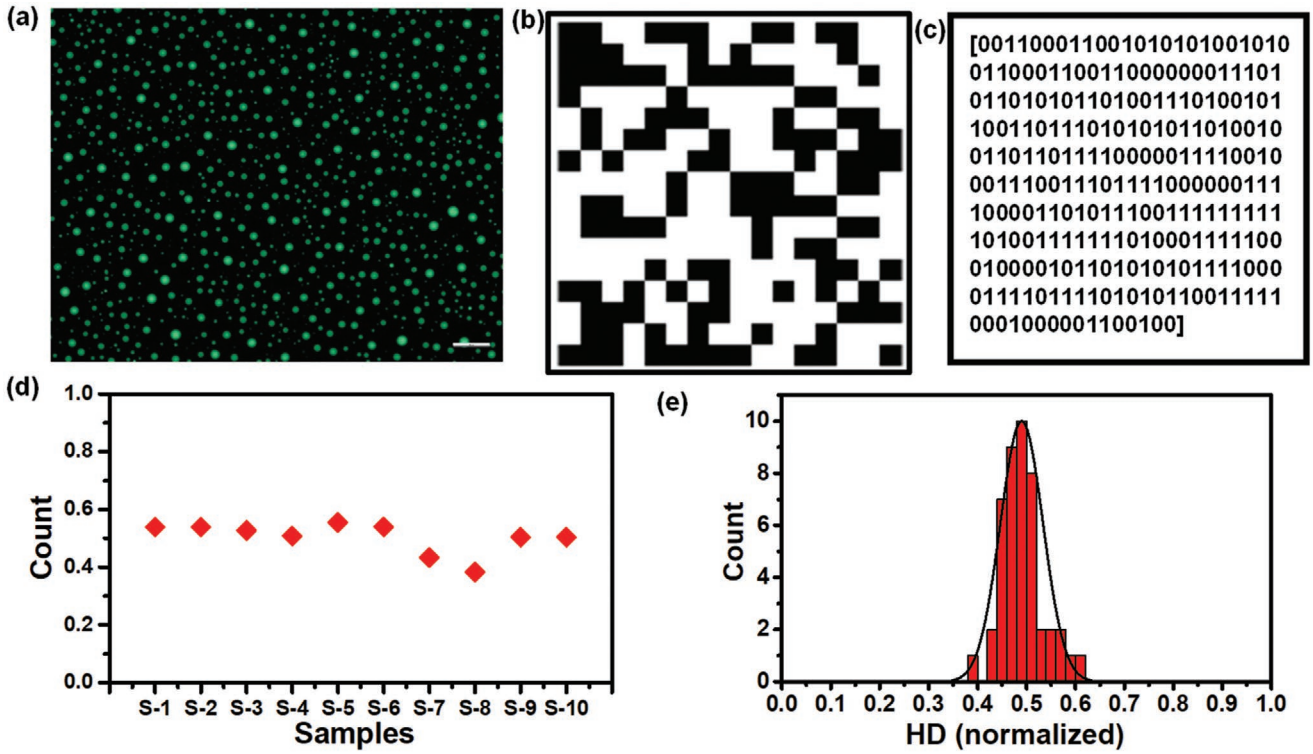

Figure 4. Key generation and extraction of PUF parameters. a) Representative fluorescence microscopy image used in the PUF analysis. b,c) Binarization and size reduction of images for generation of a security key. d) Uniformity of bits obtained from 10 samples. e) Distribution of Hamming distances for keys generated from 10 samples. Gaussian fitting is shown with the black curve. The OLE-PUF was generated by spin-coating a 0.2 wt.% solution of *f*-OSC on the PS-grafted substrate.

The fluorescence microscopy images were taken using different exposure times resulted in keys with intra-chip Hamming distance[64] values very close to zero (Table S2, Supporting Information). This capability is important, for example, in the authentication of a product at different locations throughout the supply chain. Markers can be defined on top of the OLE-PUF by physical vapor deposition of metals through a stencil mask. Such markers enable addressable sites for the authentication process (Figure S11, Supporting Information).

Despite all promising results demonstrated herein for the current *f*-OSC-based OLE-PUFs on PS-grafted silicon substrates, practical applications would require several characteristics including the ambient atmosphere processing/stability, adaptability to existing objects, resistance against ambient mechanical abrasion and water/humidity, and applicability to substrates of varying degrees of surface energy and flexibility. To this end, as shown in **Figure 5**, we have fabricated and characterized additional OLE-PUFs. First, the entire process including thermal annealing was performed in the ambient atmosphere, and excellent OLE-PUF domains, with similar properties to those fabricated under nitrogen, were obtained (Figure 5a). The thin-layer chromatography characterization of the molecular domains on the thermally annealed OLE-PUFs confirmed a robust molecular structure for 2EHO-TPA-CNPE (Figure S12, Supporting Information). The ambient atmosphere processing could greatly improve the applicability of the present OLE-PUFs. On the other hand, one would think that the relatively high surface energy (contact angle ≈ 95° and $\gamma \approx$ 41.1 mJ m^{-2}) of the end-grafted PS layer is the main thermodynamic driving force for the observed dewetting process, as we have recently seen in polymer films.[53] Thanks to the great structural mobility, flexible alkyl chains, and amorphous microstructure of the current small molecule, perfect dewetting with randomly positioned features was formed also on a freshly cleaned silicon substrate (contact angle ≈ 0° showing a high surface energy) (Figure 5b). In this case, the thermal annealing was performed in the ambient atmosphere at the same temperature (170 °C). To further take advantage of the ability to form random features on substrates of varying chemical structures and surface energies, we prepared OLE-PUFs on a flexible and transparent poly(vinyl chloride) substrate via ambient atmosphere spin-coating/thermal annealing, which again gave excellent results (Figure 5c). This kind of flexible substrates could be attached to flexible goods such as credit cards or future flexible (opto) electronic devices. We note that spin-coating may be unfeasible in certain cases, particularly when it is undesirable to coat the whole object. To this end, as shown in Figure 5d, we have demonstrated that drop-casting/thermal annealing allows for the generation of OLE-PUFs directly on goods. It is worth noting that solid-state dewetting is known to be influenced by the roughness of the substrate.[66] This behavior could be exploited in future studies to fabricate good specific PUFs. Finally, contact with humidity/water and mechanical abrasion due to ambient (micro)particles (e.g., dust, dirt, and sand) exposure is unavoidable in real-world samples, and security labels should survive such conditions. For this purpose, we used sand particles in which OLE-PUF is physically moved around and then washed the sample with water under sonication (Figure 5e). The fluorescence microscopy images (see Figure S13, Supporting Information for unmagnified images following cleaning) confirm that the OLE-PUF retains its functionality. The OLE-PUF was remarkably stable and could be authenticated after

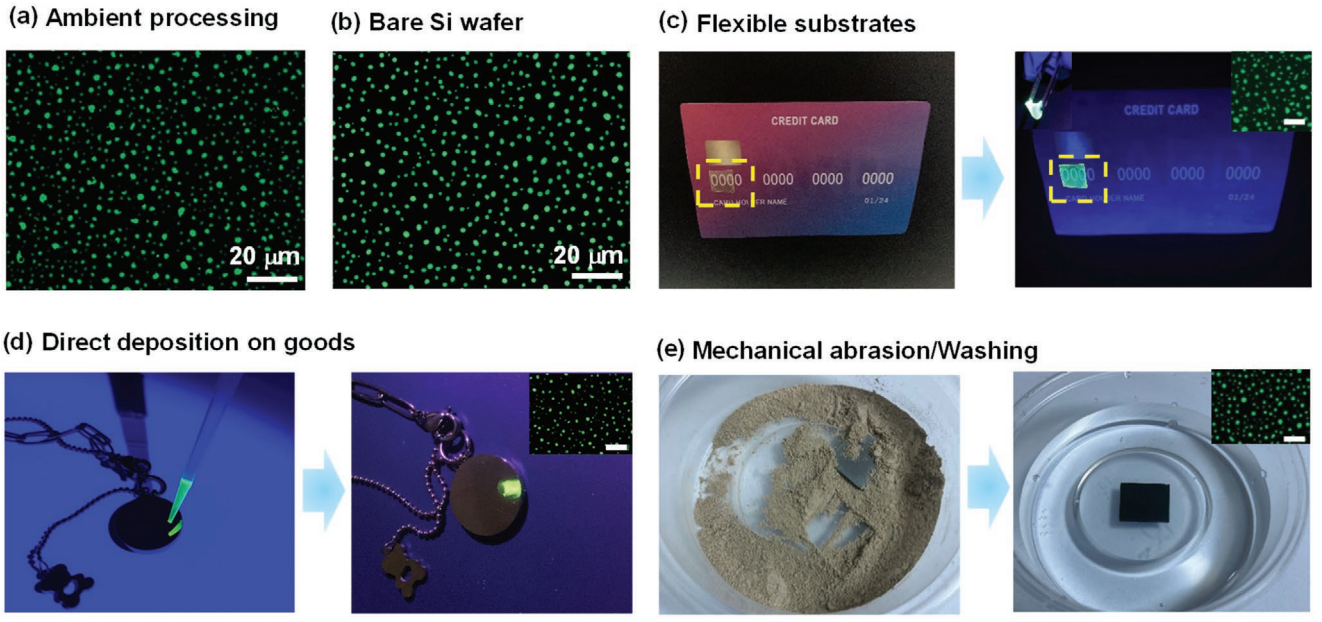

Figure 5. Enabling characteristics for practical applications. a,b) Fluorescence microscopy images of OLE-PUFs fabricated via ambient atmosphere processing and using a bare silicon substrate without an end-grafted PS layer. c) Demonstration of using a flexible plastic substrate. The OLE-PUF was formed on a flexible poly(vinyl chloride) film with a thickness of ≈280 µm. d) Direct deposition by drop-casting followed by thermal annealing allows for the generation of OLE-PUF on goods. e) The OLE-PUF is sufficiently robust to survive mechanical abrasion and washing in water under sonication. The scale bars in the inset images are 20 µm.

9 months of ambient atmosphere storage (Figure S10, Supporting Information). OLE-PUF retained its fluorescence after thermal treatment performed at 50 °C in the ambient atmosphere for 1h (Figure S14, Supporting Information), suggesting its potential use in goods encountering different temperatures around the world. TLC analysis also confirmed that the OLE-PUFs exposed to thermal treatment (50 °C for 1h) retained their chemical stability (Figure S15, Supporting Information). An additional consideration for PUFs, is tampering, which relates to unauthorized access to the system. An ideal PUF should be tamper resistant and also indicate the tampering attempt.[67–68] The dis-continuous nature consisting of discrete domains and the ability to directly form on goods of interest makes it challenging, if not impossible, to physically remove OLE-PUF without damaging the features. Tampering with more complicated means need to be investigated prior to practical validation of the proposed material system. All these capabilities demonstrated herein strongly encourage the practical fabrication and use of the 2EHO-TPA-CNPE-based OLE-PUFs.

We performed additional experiments to probe the photostability of the OLE-PUF. In a first challenge, 100 fluorescence microscopy images were captured from the identical location. This experiment simulates 100 times read-out of OLE-PUF. Figure S16a, Supporting Information presents representative fluorescence images taken after different numbers of consecutive imaging. These images qualitatively show the photostability of OLE-PUF. The images taken at identical conditions were analyzed and the intensity of fluorescence as a function of the number of images was plotted in Figure S16b, Supporting Information. The fluorescence intensity from the randomly positioned domains was higher than 90% of the initial value. In the second experiment, OLE-PUF was exposed to UV light in the ambient atmosphere for 1 h (wavelength of 365 nm and excitation power of 3 W). The fluorescence microscopy images (Figure S17, Supporting Information) of the domains were nearly identical following the UV light exposure. TLC analysis also confirmed that the OLE-PUF exposed to continuous UV-light retain its chemical stability (Figure S15, Supporting Information).

3. Conclusion

Our study has demonstrated a novel approach for the design and facile fabrication of OLE-PUFs based on a solution-processable highly fluorescent green-emissive oligo(*p*-phenyleneethynylene) molecule, 2EHO-TPA-CNPE. All ambient atmosphere-processed OLE-PUFs with excellent uniformity (0.50), uniqueness (0.49), and randomness ($p > 0.01$) were created by employing a spin-coating process followed by one-step thermal annealing (5 min). Spin-coating on low-/high-energy silicon surfaces and flexible substrates, and direct drop-casting on goods all yielded great OLE-PUF characteristics. While the random positioning of molecular domains generated the unclonable surface, the unique photophysical and structural properties formed the basis for the additional security layers (i.e., fluorescence profile, excited-state decay dynamics, Raman mapping/spectrum, and Infrared spectrum) for multiplex encoding. The size and spacing of the random features were found to depend on the film thickness and thermal annealing conditions. The amorphous microstructure of the *f*-OSC domains, enabled by the π-structure employing swallow-tailed 2-ethylhexyloxy chains and triphenylamine end-units, greatly contributes to the randomization process. The current OLE-PUFs immersed in water and exposed to mechanical abrasion by sand retained their functionality. The proposed materials and processing techniques are compatible with manufacturing routes used for the fabrication of electronic devices in the semiconductor industry. The findings presented herein clearly demonstrate that *f*-OSCs have a great potential to become a key player in the development of new-generation PUFs. This potential is not only due to its facile fabrication methodology, but also due to unique advantages of small molecules such as structural versatility, ease of synthesis/purification, high batch-to-batch reproducibility, solution-processability, and great tuning ability of their physicochemical/optoelectronic/spectroscopic properties. The future studies may include some molecular engineering perspectives focusing on modulating the π-conjugation length and the functional units to tune photoluminescence characteristics, improving photostability or tailoring alkyl chains to further decrease the dewetting temperature. From a *f*-OSC materials development perspective for future OLE-PUFs, we note that the side (hetero)aromatic units are introduced in the final step of oligo(*p*-phenyleneethynylene) synthesis, and they can directly tune the physicochemical/photophysical properties. This tunability could open new avenues towards great structural and properties versatility, all of which could provide the parametric support to bring in the required strong security barrier, including high-level trade secret molecules. Also, several host matrices with varied dielectric constants and polarities could be employed, into which the current 2EHO-TPA-CNPE molecule could be doped to yield tuned excitonic properties and emissive electronic transitions. Finally, solvent annealing[69] can also be used to facilitate the dewetting of organic materials for room temperature fabrication of PUFs.

4. Experimental Section

Preparation of Polystyrene-Grafted Substrates: Hydroxyl-terminated polystyrene (Polymer Source Inc.) with a molecular weight of 22 000 g mol^{-1} was used. Prior to the deposition of the polymer, the silicon substrates were cleaned through a UV ozone treatment for 20 min. The deposition of the polymer was performed by spin-coating 2% (w/w) solutions of hydroxyl-terminated polystyrene in toluene (Sigma-Aldrich) at 4000 rpm for 30 s. The grafting was achieved by heating the substrate at 250 °C in an argon-filled glovebox for 5 min. The excess and unreacted polymeric material were then removed by washing in toluene. The substrates were ready for the deposition of the *f*-OSC material after drying with nitrogen.

Deposition of f-OSC Material and Formation of Unclonable Surfaces: Highly efficient, green emissive 1,4-bis((4"-diphenylamino-3-cyano-[1,1" biphenyl] -4-yl) ethynyl) -2,5-bis (2-ethylhexyloxy)benzene (2EHO-TPA-CNPE) molecule was synthesized following a previous study.[54] Solutions of 2EHO-TPA-CNPE were prepared in chloroform (Sigma-Aldrich) by instant dissolution at concentrations of 0.1%, 0.2% and 0.4% (w/w). The deposition of thin-films was performed in the ambient atmosphere by spin-coating at 1200 rpm for 40 s. After spin-coating, the thin-films were annealed by heating the substrate in an argon-filled glovebox or in the ambient atmosphere for 5 min. Unless otherwise stated, the temperature of annealing was 170 °C.

Characterization: Optical and fluorescence images were taken by using a ZEISS Axio Imager 2 microscope. The fluorescence microscopy images were taken by a filter cube of GFP (S65T) with an emission wavelength of 525–540 nm. The morphology of the surface was acquired using a Zeiss EVO LS10 brand SEM microscope at 25 kV. The chemical composition of the surface was probed using an energy dispersive X-ray (EDX) detector (XFlash 6110, Bruker) connected to the SEM. The topography of the surfaces was analyzed by scanning an area with a size of 50 µm × 50 µm using an atomic force microscope (AFM, VEECO MULTIMODE 8). X-ray diffraction (XRD) measurements, were made via an X-ray diffractometer (Bruker AXS D8) using a Cu K-α source with an omega angle of 0.5° at 25 °C at a scanning step of 0.1° for 2θ = 2–40°. Raman spectra and Raman mapping images were taken using a laser with a wavelength of 532 nm, at a power of 0.1 mW power with a confocal Raman spectrometer (WITec Alpha300 M+) integrated with a fine focusing microscope. Infrared spectrum was obtained using a PerkinElmer 400 Fourier transform infrared spectrometer with a MIRacle attenuated total reflection accessory. Photoluminescence (PL) measurements were performed using an Agilent-Cary Eclipse fluorescence spectrophotometer. Fluorescence lifetime measurements were taken using the Pico Quant FluoTime 200 equipped with a 375 nm pulsed laser diode.

PUF Performance Analysis: All images were processed using MATLAB software. First, the images were converted from the RGB color space to the LAB color space. The images were then converted to gray scale. The images were then processed using inverting, dehazing and denoising algorithms. The images were then binarized. Following binarization, 1- and 0-bits refer to green fluorescent and dark regions, respectively. From these binary security keys, uniformity, uniqueness and *p*-values were calculated using a code prepared in MATLAB. The marker was fabricated by physical vapor deposition of gold using a sputter-coater through a stencil mask made of steel. The stencil mask was prepared by laser writing.

Stability Experiments: For the photostability experiments, successive fluorescence microscopy images were taken at the same position using an exposure time of 2000 ms. 100 images were taken. The fluorescence intensity from the randomly positioned domains was measured using the ZEN Blue Lite software of the ZEISS Axio Imager 2 microscope. For the UV stability, OLE-PUF was exposed to UV light with a wavelength of 365 nm with a power of 3 W. Thermal stability experiments were performed by placing silicon substrate with the OLE-PUF on a hot-plate set at a temperature of 50 °C for 1h. The sample was removed from the hot-plate at the end of the duration.

Supporting Information

Supporting Information is available from the Wiley Online Library or from the author.

Acknowledgements

This work was supported by the Research Fund of the Erciyes University (Project Number FDS-2020-9706). M.S.O. and H.U. acknowledge partial support from The Science Academy, Turkey through the Young Scientist Award Program.

Conflict of Interest

The authors declare no conflict of interest.

Data Availability Statement

The data that support the findings of this study are available from the corresponding author upon reasonable request.

Keywords

data encoding, dewetting, fluorescence, organic semiconductors, physically unclonable functions

Received: August 29, 2021
Revised: November 17, 2021
Published online:

[1] C. Fink, K. E. Maskus, Y. Qian, *World Bank Res. Obs.* **2016**, *31*, 1.
[2] A. Wali, A. Dodda, Y. Wu, A. Pannone, L. K. R. Usthili, S. K. Ozdemir, I. T. Ozbolat, S. Das, *Commun. Phys.* **2019**, *2*, 39.
[3] P. Tuyls, B. Škorić, in *Security, Privacy, and Trust in Modern Data Management*, Springer, Berlin **2007**, p. 133.
[4] S. Pekdemir, H. H. Ipekci, M. Serhatlioglu, C. Elbuken, M. S. Onses, *J. Colloid Interfaces Sci.* **2020**, *584*, 11.
[5] Y. Liu, S. Liang, C. Yuan, A. Best, M. Kappl, K. Koynov, H. J. Butt, S. Wu, *Adv. Funct. Mater.* **2021**, *31*, 2103908.
[6] R. Pappu, B. Recht, J. Taylor, N. Gershenfeld, *Science* **2002**, *297*, 2026.
[7] Y. Gao, S. F. Al-Sarawi, D. Abbott, *Nat. Electron.* **2020**, *3*, 81.
[8] T. McGrath, I. E. Bagci, Z. M. Wang, U. Roedig, R. J. Young, *Appl. Phys. Rev.* **2019**, *6*, 011303.
[9] M. Ibrar, S. E. Skrabalak, *Small Struct.* **2021**, *2*, 2100043.
[10] W. Chen, B. Javidi, X. Chen, *Adv. Opt. Photonics* **2014**, *6*, 120.
[11] B. C. Grubel, B. T. Bosworth, M. R. Kossey, H. Sun, A. B. Cooper, M. A. Foster, A. C. Foster, *Opt. Express* **2017**, *25*, 12710.
[12] Y. Du, S. Jothibasu, Y. Zhuang, C. Zhu, J. Huang, *J. Lightwave Technol.* **2017**, *35*, 4634.
[13] R. Horstmeyer, B. Judkewitz, I. M. Vellekoop, S. Assawaworrarit, C. Yang, *Sci. Rep.* **2013**, *3*, 3543.
[14] Z. Yao, T. Mauldin, G. Hefferman, Z. Xu, M. Liu, T. Wei, *Appl. Opt.* **2019**, *58*, 6211.
[15] B. R. Anderson, R. Gunawidjaja, H. Eilers, *Phys. Rev. A* **2015**, *91*, 063802.
[16] B. Škorić, A. P. Mosk, P. W. Pinkse, *Int. J. quantum Inf.* **2013**, *11*, 1350041.
[17] H. Eilers, B. R. Anderson, R. Gunawidjaja, "*Optical Signatures of Disordered Materials for Authentication Applications*," in Frontiers in Optics 2014, OSA Technical Digest (online) (Optical Society of America, 2014), paper FTh3C.6, **2014**.
[18] R. B. JD, R. Cowburn, A. Jausovec, D. Petit, P. Seem, G. Xiong, D. Atkinson, K. Fenton, D. Allwood, M. Bryan, *Nat., Brief Commun.* **2005**, *436*, 475.
[19] R. Cowburn, *Contemp. Phys.* **2008**, *49*, 331.
[20] B. Škorić, *Int. J. Quantum Inf.* **2012**, *10*, 1250001.
[21] S. A. Goorden, M. Horstmann, A. P. Mosk, B. Škorić, P. W. Pinkse, *Optica* **2014**, *1*, 421.
[22] E. Burzurí, D. Granados, E. M. Perez, *ACS Appl. Nano Mater.* **2019**, *2*, 1796.
[23] A. F. Smith, P. Patton, S. E. Skrabalak, *Adv. Funct. Mater.* **2016**, *26*, 1315.
[24] J. E. Villegas, B. Paredes, M. Rasras, *Opt. Express* **2021**, *29*, 32020.
[25] J. D. Smith, M. A. Reza, N. L. Smith, J. Gu, M. Ibrar, D. J. Crandall, S. E. Skrabalak, *ACS Nano* **2021**, *15*, 2901.
[26] V. Caligiuri, A. Patra, M. P. De Santo, A. Forestiero, G. Papuzzo, D. M. Aceti, G. E. Lio, R. Barberi, A. De Luca, *ACS Appl. Mater. Interfaces* **2021**, *13*, 49172.
[27] Q. Li, F. Chen, J. Kang, J. Su, F. Huang, P. Wang, X. Yang, Y. Hou, *Adv. Funct. Mater.* **2021**, *31*, 2010537.
[28] H. J. Bae, S. Bae, C. Park, S. Han, J. Kim, L. N. Kim, K. Kim, S. H. Song, W. Park, S. Kwon, *Adv. Mater.* **2015**, *27*, 2083.
[29] Y. W. Hu, T. P. Zhang, C. F. Wang, K. K. Liu, Y. Sun, L. Li, C. F. Lv, Y. C. Liang, F. H. Jiao, W. B. Zhao, *Adv. Funct. Mater.* **2021**, 2102108.

[30] A. Abdollahi, H. Roghani-Mamaqani, B. Razavi, M. Salami-Kalajahi, *ACS Nano* **2020**, *14*, 14417.
[31] Y. H. Zheng, C. Jiang, S. H. Ng, Y. Lu, F. Han, U. Bach, J. J. Gooding, *Adv. Mater.* **2016**, *28*, 2330.
[32] M. R. Carro-Temboury, R. Arppe, T. Vosch, T. J. Sørensen, *Science advances* **2018**, *4*, e1701384.
[33] R. Arppe-Tabbara, M. Tabbara, T. J. Sørensen, *ACS Appl. Mater. Interfaces* **2019**, *11*, 6475.
[34] Y. Liu, F. Han, F. Li, Y. Zhao, M. Chen, Z. Xu, X. Zheng, H. Hu, J. Yao, T. Guo, *Nat. Commun.* **2019**, *10*, 2409.
[35] Y. Liu, Y. Zheng, Y. Zhu, F. Ma, X. Zheng, K. Yang, X. Zheng, Z. Xu, S. Ju, Y. Zheng, *ACS Appl. Mater. Interfaces* **2020**, *12*, 39649.
[36] J. W. Leem, M. S. Kim, S. H. Choi, S.-R. Kim, S.-W. Kim, Y. M. Song, R. J. Young, Y. L. Kim, *Nat. Commun.* **2020**, *11*, 1.
[37] Y. Fan, C. Zhang, Z. Gao, W. Zhou, Y. Hou, Z. Zhou, J. Yao, Y. S. Zhao, *Adv. Mater.* **2021**, *33*, 2102586.
[38] F. Chen, Q. Li, M. Li, F. Huang, H. Zhang, J. Kang, P. Wang, *Chem. Eng. J.* **2021**, *411*, 128350.
[39] H. Usta, D. Kim, R. Ozdemir, Y. Zorlu, S. Kim, M. C. Ruiz Delgado, A. Harbuzaru, S. Kim, G. Demirel, J. Hong, *Chem. Mater.* **2019**, *31*, 5254.
[40] R. Ozdemir, K. Ahn, I. Deneme, Y. Zorlu, D. Kim, M.-G. Kim, H. Usta, *J. Mater. Chem. C* **2020**, *8*, 15253.
[41] J. Oh, D. Baek, T. K. Lee, D. Kang, H. Hwang, E. M. Go, I. Jeon, Y. You, C. Son, D. Kim, *Nat. Mater.* **2021**, *20*, 385.
[42] H. Bronstein, C. B. Nielsen, B. C. Schroeder, I. McCulloch, *Nat. Rev. Chem.* **2020**, *4*, 66.
[43] S. R. Forrest, M. E. Thompson, *Chem. Rev.* **2007**, *107*, 923.
[44] H. Usta, A. Facchetti, T. J. Marks, *Acc. Chem. Res.* **2011**, *44*, 501.
[45] R. Capelli, S. Toffanin, G. Generali, H. Usta, A. Facchetti, M. Muccini, *Nat. Mater.* **2010**, *9*, 496.
[46] P. Zhu, S. Li, X. Jiang, Q. Wang, F. Fan, M. Yan, Y. Zhang, P. Zhao, J. Yu, *Anal. Chem.* **2019**, *91*, 10320.
[47] C. H. Oh, H. J. Shin, W. J. Nam, B. C. Ahn, S. Y. Cha, S. D. Yeo, presented at SID Symposium Digest of Technical Papers **2013**.
[48] J. Feng, W. Wen, X. Wei, X. Jiang, M. Cao, X. Wang, X. Zhang, L. Jiang, Y. Wu, *Adv. Mater.* **2019**, *31*, 1807880.
[49] D. Okada, Z.-H. Lin, J.-S. Huang, O. Oki, M. Morimoto, X. Liu, T. Minari, S. Ishii, T. Nagao, M. Irie, *Mater. Horiz.* **2020**, *7*, 1801.
[50] R. Ozdemir, D. Choi, M. Ozdemir, H. Kim, S. T. Kostakoğlu, M. Erkartal, H. Kim, C. Kim, H. Usta, *ChemPhysChem* **2017**, *18*, 850.
[51] H. Ebata, T. Izawa, E. Miyazaki, K. Takimiya, M. Ikeda, H. Kuwabara, T. Yui, *J. Am. Chem. Soc.* **2007**, *129*, 15732.
[52] C. V. Thompson, *Annu. Rev. Mater. Res.* **2012**, *42*, 399.
[53] N. Torun, I. Torun, M. Sakir, M. Kalay, M. S. Onses, *ACS Appl. Mater. Interfaces* **2021**, *13*, 11247.
[54] H. Usta, D. Alimli, R. Ozdemir, E. Tekin, F. Alkan, R. Kacar, A. G. Altas, S. Dabak, A. G. Gürek, E. Mutlugun, A. F. Yazici, A. Can, *J. Mater. Chem. C* **2020**, *8*, 8047.
[55] G. Reiter, *Langmuir* **1993**, *9*, 1344.
[56] N. Deneke, A. L. Chau, C. S. Davis, *Soft Matter* **2021**, *17*, 863.
[57] S. Kowarik, A. Gerlach, S. Sellner, L. Cavalcanti, F. Schreiber, *Adv. Eng. Mater.* **2009**, *11*, 291.
[58] A. Facchetti, *Mater. Today* **2007**, *10*, 28.
[59] A. Facchetti, *Chem. Mater.* **2011**, *23*, 733.
[60] H. Sun, X. Guo, A. Facchetti, *Chem* **2020**, *6*, 1310.
[61] S. Pekdemir, I. Torun, M. Sakir, M. Ruzi, J. A. Rogers, M. S. Onses, *ACS Nano* **2020**, *14*, 8276.
[62] H. Usta, D. Alimli, R. Ozdemir, S. Dabak, Y. Zorlu, F. Alkan, E. Tekin, A. Can, *ACS Appl. Mater. Interfaces* **2019**, *11*, 44474.
[63] M. Ozdemir, D. Choi, Y. Zorlu, B. Cosut, H. Kim, C. Kim, H. Usta, *New J. Chem.* **2017**, *41*, 6232.
[64] A. Maiti, V. Gunreddy, P. Schaumont, in *Embedded Systems Design with FPGAs*, Springer, New York **2013**, p. 245.
[65] L. E. Bassham III, A. L. Rukhin, J. Soto, J. R. Nechvatal, M. E. Smid, E. B. Barker, S. D. Leigh, M. Levenson, M. Vangel, D. L. Banks, A. Heckert, J. Dray, S. A. Vo, *Natl. Inst. Stand. Technol.* **2010**.
[66] P. Volodin, A. Kondyurin, *J. Phys. D: Appl. Phys.* **2008**, *41*, 065307.
[67] B. R. Anderson, R. Gunawidjaja, H. Eilers, *Appl. Opt.* **2017**, *56*, 2863.
[68] B. P. Williams, K. A. Britt, T. S. Humble, *Phys. Rev. Appl.* **2016**, *5*, 014001.
[69] H. Yamagishi, T. Matsui, Y. Kitayama, Y. Aikyo, L. Tong, J. Kuwabara, T. Kanbara, M. Morimoto, M. Irie, Y. Yamamoto, *Polymers* **2021**, *13*, 269.